UV Raman Microspectroscopy: Spectral and Spatial Selectivity with Sensitivity and Simplicity

VASIL PAJCINI, CALUM H. MUNRO, RICHARD W. BORMETT, ROBERT E. WITKOWSKI, and SANFORD A. ASHER*

Department of Chemistry, University of Pittsburgh, Pittsburgh, Pennsylvania 15260

The high sensitivity, selectivity, spatial resolution, and ease of operation of UV Raman microspectroscopy is demonstrated with the use of a new highly efficient UV Raman microspectrometer with excitation at 244 nm. Single spectrograph dispersion combined with special new filters for the rejection of Rayleigh scattering improves the throughput efficiency by a factor of approximately 4 in comparison to a triple-stage spectrograph. The instrument has a spatial resolution of approximately 3 μm × 9 μm in the lateral (X–Y) plane, and 10 μm or less in the axial (Z) plane. UV resonance Raman spectra of nucleic acids are selectively excited from spatially resolved areas of a single paramecium by using low continuous-wave (cw) excitation powers and short accumulation times to minimize sample damage. High signal-to-noise Raman spectra are excited from spatially resolved areas of chemical-vapor-deposited (CVD) diamond films. We demonstrate, for the first time, the ability to probe the spatial distribution of the nondiamond carbon impurities in CVD diamond films. The amorphous carbon band at ~ 1553 cm^{-1} is resolved from the normally broad ~ 1600-cm^{-1} nondiamond carbon band.

Index Headings: **UV Raman spectroscopy; Microspectroscopy; Diamond; Eukaryotic cell; DNA; Spatial resolution; High efficiency.**

INTRODUCTION

During the last 20 years, visible Raman microspectroscopy and Raman imaging have been utilized successfully in chemical analysis, geology, and industrial quality control[1–8] and in biological studies including the examination of single cells.[9] In parallel, UV resonance Raman spectroscopy (UVRRS) has emerged as a highly sensitive and selective technique for studying the vibrational spectra of molecules which have electronic transitions in the region between 180 and 300 nm,[10–31] with the development of instrumentation capable of excitation in this region.[32]

The high selectivity and sensitivity of UVRRS permit important analytical applications. We have demonstrated the ability to selectively examine individual species in complex matrices.[14–15,20] For example, excitation coincident with the narrow UV absorption bands of polycyclic aromatic hydrocarbons (PAHs) enhances the Raman cross section by a factor of approximately 10^8 and thus enables the examination of low concentrations of these analytes in complex environments, such as coal-derived liquids and petroleum fractions, and even intercalated between DNA base pairs.[22]

The ability to combine the high sensitivity and selectivity of UVRRS with the ease of operation and spatial resolution of visible Raman microscopy or microspectroscopy is highly desirable. However, until recently the excitation sources utilized for UV Raman measurements were inappropriate for UV Raman microspectroscopy. Frequency-doubled YAG or XeCl excimer lasers with pulse widths of approximately 10 ns and low repetition rates (<300 Hz) were used to pump near-UV or visible dye lasers, and the pulsed dye laser outputs were then subject to nonlinear optical processes such as frequency doubling or mixing, yielding completely tunable UV light at relatively low duty cycles and very high peak powers. Focused, these pulses readily cause dielectric breakdown in any sample, and even with diffuse focusing and low peak powers, other nonlinear optical phenomena can compete with Raman scattering. Furthermore, at peak powers which are lower still, Raman saturation phenomena can occur, which depopulate the ground state and create transient concentrations of excited-state species.[33–36] To avoid nonlinear phenomena and saturation, one should obtain pulsed Raman measurements from flowing or spinning samples using broad, defocused beams with pulse energy flux densities of less than 1 mJ/cm^2. However, less than 1% of the incident photons in the broad defocused beam are effectively used as an excitation source. This is because in a standard backscattering or 90° scattering geometry only a small spatial area of the beam spot can be imaged into the narrow slits (1–200 μm) used by high-resolution Raman spectrometers. This percentage would be further reduced significantly with the greatly increased spatial resolution of UV Raman microspectroscopy.

We have recently demonstrated the superiority of new continuous-wave (cw) argon- and krypton-ion laser sources.[14,37] These intracavity frequency-doubled ion lasers have several discrete output wavelengths between 206.5 and 257.3 nm. The ability to focus the cw argon-ion laser to a spot size that can be efficiently imaged into the spectrometer permits much higher spectral signal-to-noise (S/N) ratios. Most importantly, we have demonstrated that the cw laser can be used to examine thermally sensitive samples including strongly absorbing solid samples, and that the beam can be focused to small diameters without saturation and nonlinear phenomena and with comparatively small photodegradation of the sample. These results indicate that an efficient UV Raman microspectrometer can now be constructed.

The use of UV Raman microspectrometers has been reported for the examination of dAMP deoxymononucleotide DNA and single T47D cultured human mammary tumor cells,[38] as well as bacterial cells.[39] However, the instrumentation limitations in each study resulted in low efficiencies. For example, Sureau et al.[38] focused the laser into the sample under grazing incidence to avoid overheating or photodamage of the sample and used a low-numerical-aperture (NA = 0.2) 10× Zeiss Ultrafluar

Received 23 February 1996; accepted 3 July 1996.

* Author to whom correspondence should be sent.

0003-7028/97/5101-0081$2.00/0

objective to collected the Raman scattering. Chadha et al.[39] excited and collected the UV Raman scattering from bacterial cells in a 180° scattering geometry using a Cassagrain reflective objective, but used a triple-stage spectrograph with a low throughput efficiency of ≤3% as the dispersing system.

In this report we demonstrate for the first time the use of an efficient new UV Raman microspectrometer which enables the high sensitivity and selectivity of UV Raman spectroscopy and the spatial resolution and ease of operation of optical microscopy to be realized simultaneously.

EXPERIMENTAL

UV Raman spectra were excited with a Coherent Innova 300 intracavity frequency-doubled argon-ion laser system. Raman scattering was collected in a backscattering geometry via the microscope assembly described below and imaged into a Spex 1701 750-mm single monochromator (*f*/6.8) equipped with a 2400-groove/mm holographic grating and an EG&G PARC 1456 blue intensified photodiode array and optical multichannel analyzer. The relative efficiency of the spectrometer between 200 and 350 nm was measured with an Optronic Laboratories Inc. UV 40 calibrated spectral irradiance deuterium lamp. The absolute efficiency of the spectrometer was determined by indexing the relative efficiency to the absolute efficiency measured at ~251 nm by using a photodiode to measure the power of the ~251-nm line of the frequency-doubled argon-ion laser before and after the beam passed through the spectrometer.

Chemical-vapor-deposited (CVD) diamond films were prepared at Westinghouse Science and Technology Center in Pittsburgh, PA. Diamond films were grown on a silicon substrate by using a 1.5-kW ASTeX microwave plasma reactor with a hydrogen, methane, and oxygen input gas mixture. UV Raman spectra of the diamond film were obtained with a total accumulation time of 10 s. The 244-nm beam was focused, with a 50-mm lens, to a spot size of approximately 9 μm.

Paramecia were immobilized 20–25 min prior to examination by adding an aqueous solution of Detain™, a nontoxic, nonionic, viscoelastic slowing reagent (70 μL, 1.0% w/v; Ward's Natural Science Establishment Inc.) to the *Paramecium caudatum* culture (100 μL, cerophyll medium; Ward's Natural Science Establishment Inc.). The UV Raman spectra of the paramecium macronucleus were obtained with an excitation power of approximately 0.2 mW and a total accumulation time of 20 s. The 244-nm beam was focused, with a 100-mm lens, to a spot size of approximately 25 μm.

RESULTS AND DISCUSSION

This report describes a new UV Raman microspectrometer based on a modified Olympus BX60 series microscope. Figure 1 illustrates the optical layout of the microspectrometer.

We previously described in detail the intracavity frequency-doubled argon-ion laser used to excite the UV Raman scattering.[14] The 244-nm cw UV Raman laser beam, expanded to approximately 10 mm in diameter, is focused by using a 5- to 10-cm-focal-length lens onto the

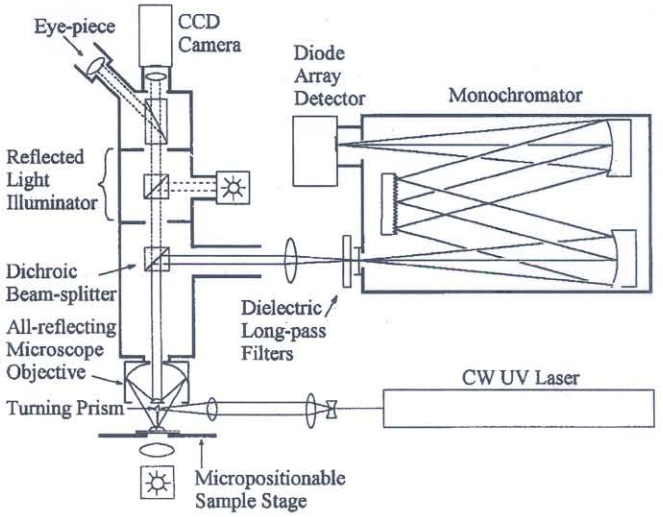

FIG. 1. Schematic diagram showing the optical layout of the UV Raman microspectrometer.

sample via a Suprasil 90° turning prism mounted directly below the Cassegrain objective. The beam can be focused to a spot size of 5–25 μm. An Opticon Corp. 36× all-reflective Cassegrain microscope objective with a back focus of 160 mm, a working distance of 10.5 mm, and an NA of 0.5 is used to collect the backscattered light. The 0.5-NA objective enables collection of scattered radiation over a large solid angle (half angle = 30°) compared with the 0.2-NA objective (half angle = 11.5°) used in a previous study.[38] The objective has a dielectric overcoated aluminum coating (Al/MgF_2). This Cassegrain objective serves as a highly efficient collection optic for the scattered radiation; collecting at *f*/1, the sample illuminated with a spot size of 5–10 μm can be imaged efficiently into the entrance slit (100–200 μm) of the monochromator (*f*/6.8).

An Omega Optical Inc. 290 DCLPO2 UV dichroic beamsplitter was used to reflect > 90% of the scattered UV light between 230 and 265 nm to the collecting optics of the monochromator and to transmit light between 300 and 2000 nm to the microscope trinocular eyepiece. The dichroic beamsplitter is mounted in a fluorescence cube module, housed in the epi-illuminator turret, which has been modified to enable the effective coupling of the scattered UV radiation into the spectrograph.

A 0.75-m single monochromator (*f*/6.8) was used as the dispersion system. Triple monochromators are normally required for stray light rejection but are notoriously inefficient; only 2–3% of the Raman scattered UV light entering the entrance slit is transferred to the detector. The advantages of using a single monochromator with holographic notch filters for the rejection of Rayleigh scattering and a holographic grating to reduce stray light from the grating have been well demonstrated for visible Raman spectroscopy and imaging. Notch filters are not currently available in the UV region. However, for the first time we demonstrate the use of dielectric longpass filters, custom constructed by Omega Optical Inc., with a transmittance of 0.01% at 244 nm and 65–80% between 252 and 262 nm. The use of two of these dielectric filters to reject the Rayleigh scattered light enables a single

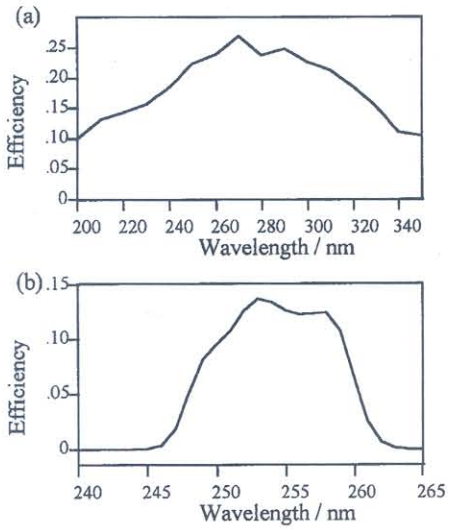

FIG. 2. Plot of the efficiency (**a**) of the 0.75-m single monochromator and detector and (*b*) of the 0.75-m single monochromator, detector, and two long-pass filters for Rayleigh rejection (244 nm) vs. wavelength.

monochromator with a holographic grating to be employed to disperse the Raman Stokes-shifted radiation.

The microscope is modified with an Olympus U-RLA epi-illuminator and universal lamp housing. We have also attached a C-mount video port to the trinocular tube to permit the use of a charge-coupled device (CCD) camera to view visible light from the sample, for example, visible fluorescence and photoluminescence bands excited by the incident 244-nm radiation.

Our Raman microscope design is unconventional since the excitation beam is introduced to the sample independently of the collected light, as opposed to the more typical epi-illumination. Our design has the advantage that the beam focal spot size and position are adjustable independently of the focusing conditions for collecting the Raman scattered light. In addition, this arrangement with the Cassegrain objective does not suffer any loss of laser beam throughput or scattered light throughput to the spectrometer. This arrangement is probably required for the deep UV excitation, since the aluminized optics and the dielectric coatings slowly degrade with time with the intense laser excitation. Further, stray light scattering from the interior microscope optics is avoided, since the excitation beam path does not pass through the microscope optics. This feature improves the spectral signal-to-noise ratios. The only disadvantage of this design is that it limits the ultimate microscope resolution, since the laser light is focused by a longer focal length lens than the microscope objective. In principle, we could achieve submicrometer resolution. We can easily modify the microscope for epi-illumination if, in the future, we wish to dramatically improve our resolution.

Efficiency. Figure 2 illustrates the efficiency of the monochromator and detector between 200 and 350 nm and the monochromator and detector combined with the dielectric longpass filters between 240 and 265 nm. The throughput efficiency of the microspectrometer is cut off near the Rayleigh scattered light at 244 nm by the dielectric longpass filters, which determine a working spectral window of approximately 247 to 261 nm. This range corresponds to a Raman Stokes-shift range of approximately 500 to 2670 cm^{-1} for 244-nm excitation.

Within this working spectral window, the absolute throughput efficiency of the microspectrometer is high in comparison to that for typical spectrometers used for UV Raman measurements. For example, the efficiency determined at 251 nm is 84% for the microscope assembly, including the Cassegrain objective and dichroic beamsplitter, 22.5% for the monochromator alone, and 10.8% for the monochromator and two long-pass filters for Rayleigh rejection. Thus, even with significant losses due to the long-pass filters, the throughput efficiency is greater than that for a triple monochromator by a factor of approximately 3 to 4 times.

Spatial Resolution. The spatial resolution of the microspectrometer is determined by the spot size of the focused laser and the spectrometer slit. The sample area illuminated with a spot size of approximately 9 μm forms an image approximately 275 μm in diameter on the entrance slit. Thus, with a slit width of 100 μm our spatial resolution in the lateral (X–Y) plane will be approximately 3 μm × 9 μm. We have also demonstrated the spatial resolution in the axial (Z) plane to be on the order of 10 μm or less. Previous studies have demonstrated that a depth resolution of 1–2 μm can be obtained by using a confocal configuration, i.e., by placing a pinhole at the back image plane of the microscope objective to block light from outside the focal plane.[4–5,9] We could adopt a confocal arrangement by introducing a pinhole and lens to achieve increased depth resolution where required.

UV Raman Microspectroscopy of Chemical-Vapor-Deposited Diamond Film. The utility of UVRRS results not only from resonance enhancement but also from the fact that fluorescence interference within the Raman spectrum does not occur for condensed-phase samples excited below 250 nm;[40] fluorescence interference from impurities is a major impediment for Raman studies utilizing near-UV, visible, or near-IR excitation. We demonstrated that diamond Raman spectra excited within or close to the diamond bandgap have dramatically improved S/N ratios, due to the lack of interfering fluorescence signals.[10] This factor allowed us to monitor the spectral differences between different nondiamond carbon species. We were also able to observe for the first time the carbon–hydrogen (C–H) stretching vibrations of the nondiamond components of the CVD diamond films and to examine the intensity and frequency of the third-order phonon bands of diamond. Furthermore, we were able to detect and quantify different nondiamond carbon species in the CVD diamond films. We demonstrated that the intensity ratio of the UV-excited Raman bands assigned to the C–H stretching of nondiamond impurities (2930 cm^{-1}) to the diamond first-order phonon band at 1332 cm^{-1} is proportional to the atomic fraction of covalently bound hydrogen in the CVD diamond films.

Figure 3 shows the (100) face of a diamond crystallite on the surface of a CVD diamond film. Figure 4 shows the UV Raman spectra of this CVD diamond film excited at 244 nm (~ 1.5 mW). The diamond UV Raman spectra were recorded with the laser spot centered on the (100) face of single diamond crystallite (Fig. 4a) or at the grain boundaries between diamond crystallites (Fig. 4b).

The absolute intensity of the diamond first-order pho-

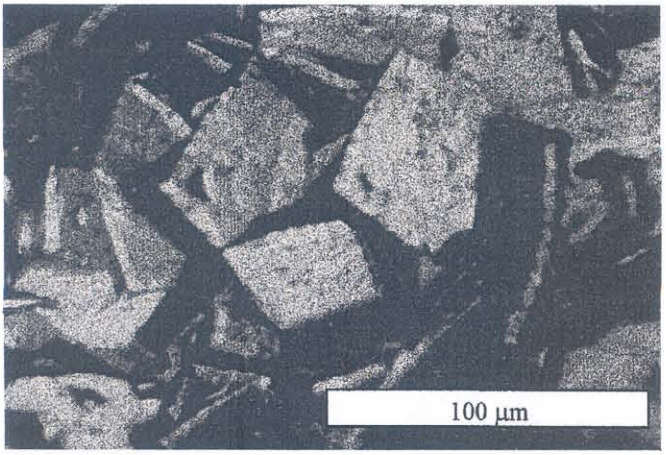

FIG. 3. CVD diamond film surface with visible epi-ilumination, viewed through the microscope attachment of the UV Raman microspectrometer, showing the (100) faces of single crystallites.

non band at 1332 cm^{-1} was approximately the same at the (100) face (Fig. 4a) and the grain boundaries (Fig. 4b). However, the UV Raman spectrum taken from the grain boundaries showed a broad band at ~ 1600 cm^{-1}, assignable to nondiamond carbon impurities. This band was not present in the spectrum from the (100) crystallite face. These results demonstrate the ability to determine the spatial distribution of nondiamond impurities in CVD diamond films.

Our previous study of the oxidative degradation of CVD diamond films showed that upon oxidation the intensity of the broad nondiamond carbon band at ~ 1550 cm^{-1} and the C–H stretching band of the nondiamond components at 2930 cm^{-1} decreased with respect to the diamond first-order phonon band, but that the initial rate of decrease was significantly greater for the 1550-cm^{-1} band than for the 2930-cm^{-1} band.[10] These results indicate that nondiamond carbon species are oxidized in preference to diamond. They also suggest that more than one nondiamond carbon impurity is present in CVD diamond films.

Figure 4b illustrates that, using UV Raman microspectrometry, we can resolve underlying components of the nondiamond carbon band. In this instance, a sharp low-energy feature, fitted to the ~ 1553-cm^{-1} amorphous carbon band, is resolved from the broad ~ 1603-cm^{-1} nondiamond carbon band (fit correlation, $R^2 = 0.97$). In other instances, the sharp ~ 1580 cm^{-1} graphite band dominates the nondiamond carbon band. The limited spatial area probed enables us to speciate the different nondiamond carbon species which make up the normally broad nondiamond carbon band.

In addition to the observation of high signal-to-noise UV Raman spectra, the visible emission from different spatially resolved regions of the CVD diamond film was recorded with a color CCD camera attached to the trinocular of the microscope. The room-temperature visible photoluminescence spectrum from a single diamond crystallite was excited at 244 nm and measured with the microspectrometer. Focusing the 244-nm beam at the grain boundaries excites the intense blue and green luminescence, which is generally observed in bulk measurements of diamond films and which interferes with the visible Raman measurements. However, Fig. 5 shows that red photoluminescence (575 nm; 2.15 eV) is excited by focusing the beam at the (100) face, where no significant nondiamond carbon impurities were observed. The 575-nm emission band can be observed in either cathodoluminescence or photoluminescence. There is no accepted model for the defect center associated with this band, but it is produced in all diamonds by irradiation followed by annealing (900–1100 K).[41] In bulk measurements that do not probe spatially limited areas, excitation over large areas results in emission which is dominated by the intense blue/green luminescence from nondiamond carbon species.

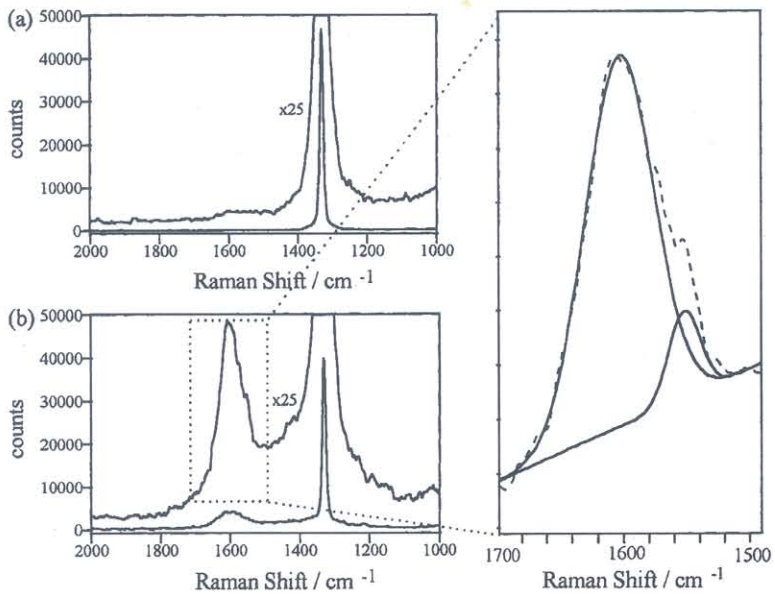

FIG. 4. Raman spectra from CVD diamond film (**a**) at the (100) face of a single crystallite and (**b**) at the interstices between diamond crystallites (244 nm; ~ 1.5-mW average power; 10-s total accumulation time; 100-μm entrance slit).

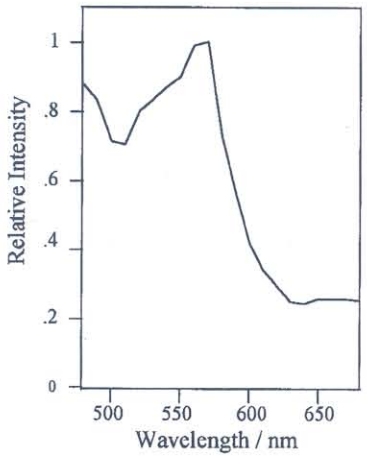

FIG. 5. Red photoluminescence (575 nm; 2.15 eV) excited by focussing the beam on the (100) face of a CVD diamond crystallite (244 nm; 100 mW average power; 100-μm entrance slit).

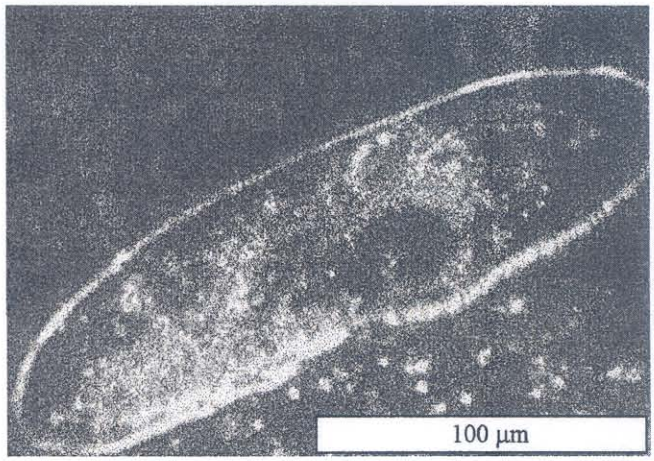

FIG. 6. Visible image of paramecium viewed through the microscope attachment of the UV Raman microspectrometer. The dark approximately spherical area to the immediate right of center is the macronucleus.

UV Raman Microspectroscopy of Biological Samples. We have also examined the potential of UV Raman microspectroscopy for the examination of biological samples. For example, Fig. 6 shows a live paramecium viewed through the microscope using a CCD camera. The macronucleus is on the order of 25–30 μm in diameter and is clearly visible (dark approximately spherical area in Fig. 5). Figure 7a illustrates the Raman spectrum probed within the macronucleus of a single paramecium, while Fig. 7b shows the resonance Raman spectrum of calf-thymus DNA. The high collection and throughput efficiency of the microspectrometer, the low excitation powers (0.2 mW), and the short accumulation times (20 s) yield spectra with high S/N ratios while causing only minimal degradation to these biological systems.

The bands from calf-thymus DNA and from the paramecium macronucleus observed between 1240 and 1700 cm^{-1} are assigned to nucleic acid base vibrations.[42] These bands experience significant resonance enhancement from the nucleic acid $\pi^* \leftarrow \pi$ transitions responsible for the broad absorption bands between 236 and 282 nm in the spectrum of DNA.[43] The principal Raman band of calf-thymus DNA at 1484 cm^{-1} is due to the overlapping bands of adenine at 1482 cm^{-1} and guanine at 1480–1485 cm^{-1}.[42,44] The broad bands at 1333 and 1575 cm^{-1} with shoulders at approximately 1315 and 1610 cm^{-1} derive from different ring vibrations of adenine residues[44] and the overlap of the vibrations of bases of poly(A) and poly(G).[44] A small band at 1412 cm^{-1} is assigned to ring vibration of poly(C).[42]

Comparison of the spectra illustrates that Raman scattering from the paramecium macronucleus is dominated by resonance-enhanced DNA bands at 1331 and 1486 cm^{-1}. The band at 1575 cm^{-1} lies under a broad band with maxima at 1585 and 1611 cm^{-1}.

The paramecium examined were approximately 5–10 μm thick. Focusing to 10 μm above or below the nucleus of the paramecium yielded spectra only from the Detain™ solution and not from DNA. However, when the focal plane of the objective was within the macronucleus, there was no observable contribution by Detain™ to the spectrum recorded. Thus, the spatial resolution of the system in the axial plane is on the order of 10 μm or less.

CONCLUSION

We have developed a new highly efficient UV Raman microspectrometer and have demonstrated the high sensitivity, selectivity, spatial resolution, and ease of operation of UV Raman microspectroscopy. Using a single spectrograph dispersion system with special new filters for rejection of the 244-nm excitation frequency improves the throughput efficiency by a factor of approximately 4 in comparison to that for a triple-stage spectrograph.

The present instrument spatial resolution is approximately 3 μm × 9 μm in the lateral (X–Y) plane, as determined by the image size passing through the limiting apertures, and 10 μm or less in the axial (Z) plane. The resolution in the axial plane can be improved where required by utilizing a confocal arrangement.

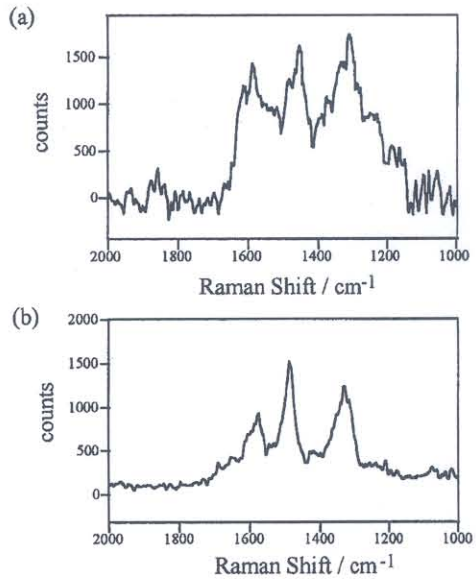

FIG. 7. Resonance Raman spectra of (**a**) paramecium macronucleus (244 nm; 0.2 mW-average power; 20-s total accumulation time) and (**b**) calf-thymus DNA (244 nm; 0.2-mW average power; 20-s total accumulation time; 150-μm entrance slit).

We demonstrated the ability to selectively excite UV resonance Raman spectra from spatially resolved areas of biological samples within the nucleus of a single cell (in particular, from DNA) using low excitation powers and short accumulation times to minimize sample damage. In addition, UV Raman microspectroscopy has enabled us for the first time to probe the spatial distribution of non-diamond carbon impurities in CVD diamond films. Furthermore, the limited spatial area probed allowed us to resolve the 1553-cm^{-1} amorphous carbon band from the normally broad nondiamond carbon band.

ACKNOWLEDGMENTS

We gratefully thank Westinghouse Science and Technology Center for providing CVD diamond films and acknowledge support from an AFOSR grant to the University of Pittsburgh Materials Research Center (F49620-95-1-0167) and from an NIH grant (R01GM30741–13).

1. J. Rosasco, E. S. Etz, and W. A. Cassatt, Appl. Spectrosc. **29,** 396 (1975)
2. M. Delhaye and P. Dhamelincourt, J. Raman Spectrosc. **3,** 33 (1975).
3. J. Rosasco, in *Advances in Infrared and Raman Spectroscopy*, R. J. H. Clark and R. E. Hester, Eds. (Heyden, London, 1980), vol. 7, p. 223.
4. P. J. Treado and M. D. Morris, Appl. Spectrosc. Rev. **29,** 1 (1994).
5. R. Tabaksblat, R. J. Meier, and B. J. Kip, Appl. Spectrosc. **46,** 60 (1992).
6. J. Barbillat, P. Dhamelincourt, M. Delhaye, and E. Da Silva, J. Raman Spectrosc. **25,** 3 (1994).
7. A. Garton, D. N. Batchelder, and C. Cheng, Appl. Spectrosc. **47,** 922 (1993).
8. K. P. J. Williams, G. D. Pitt, D. N. Batchelder, and B. J. Kip, Appl. Spectrosc. **48,** 232 (1994).
9. J. Puppels, F. F. M. De Mul, C. Otto, J. Greve, M. Robert-Nicoud, D. J. Arndt-Jovin, and T. Jovin, *Nature* **347,** 301 (1990).
10. R. W. Bormett, S. A. Asher, R. E. Witkowski, W. D. Partlow, R. Lizewski, and F. Pettit, J. Appl. Phys. **77,** 5916 (1995).
11. S. A. Asher, Ann. Rev. Phys. Chem. **39,** 537 (1988);
12. S. A. Asher, Anal. Chem. **65,** 59A (1993).
13. S. A. Asher, Anal. Chem. **65,** 201A (1993).
14. S. A. Asher, R. W. Bormett, X. G. Chen, D. H. Lemmon, N. Cho., P. Peterson, M. Arrigoni, L. Spinelli, and J. Cannon, Appl. Spectrosc. **47,** 628 (1993).
15. S. A. Asher, Anal. Chem. **56,** 720 (1984).
16. S. A. Asher, Anal. Chem. **56,** 2258 (1984).
17. R. Rumelfanger, S. A. Asher, and M. B. Perry, Appl. Spectrosc. **42,** 267 (1988).
18. C. M. Jones and S. A. Asher, J. Chem. Phys. **89,** 2649 (1988).
19. S. A. Asher, Ann. Rev. Phys. Chem. **39,** 537 (1988).
20. J. D. Getty, S. D. Westre, D. Z. Bezebeh, G. A. Barral, M. J. Burmeister, and P. B. Kelly, Appl. Spectrosc. **46,** 620 (1992).
21. P. A. Harmon and S. A. Asher, J. Chem. Phys. **93,** 3064 (199).
22. N. Cho and S. A. Asher, J. Am. Chem. Soc. **115,** 6349 (1993).
23. T. G. Spiro, G. Smulevich, and C. Su, *Biochemistry* **29,** 4497 (1990).
24. I. Harada, T. Yamagishi, K. Uchida, and H. Takeuchi, J. Am. Chem. Soc. **112,** 2443 (1990).
25. R. A. Copeland and T. G. Spiro, Biochemistry **29,** 4497 (1990).
26. S. P. A. Fodor and T. G. Spiro, J. Am., Chem. Soc. **108,** 3198, (1986).
27. W. L. Kubasek, B. Hudson, and W. Peticolas, Proc. Natl. Acad. Sci. USA **82,** 2369 (1985).
28. R. J. Sension and B. S. Hudson, J. Chem. Phys. **90,** 1377 (1989).
29. L. D. Ziegler and B. S. Hudson, J. Chem. Phys. **79,** 1134 (1983).
30. B. S. Hudson and L. C. Mayne, in *Biological Applications of Raman Spectroscopy*, T. G. Spiro, Ed. (John Wiley and Sons, New York, 1987), Vol. II, pp. 181–209.
31. B. Hudson and L. Mayne, Methods Enzymol. **130,** 331 (1986).
32. S. A. Asher, C. R. Johnson, and J. Murtaugh, Rev. Sci. Instrum. **54,** 1657 (1983).
33. C. R. Johnson, M. Ludwig, and S. A. Asher, J. Am. Chem. Soc. **108,** 905 (1986).
34. M. Ludwig and S. A. Asher, J. Am. Chem. Soc. **110,** 1005 (1988).
35. J. Teraoka, P. A. Harmon, and S. A. Asher, J. Am. Chem. Soc. **112,** 2892 (1990).
36. P. A. Harmon, J. Teraoka, and S. A. Asher, J. Am. Chem. Soc. **112,** 8789 (1990).
37. J. S. W. Holtz, R. W. Bormett, Z. Chi, N. Cho, V. Pajcini, S. A. Asher, M. Arrogoni, P. Owen, and L. Spinelli, Appl. Spectrosc., paper in press.
38. Sureau, L. Chinsky, C. Amirand, J. P. Ballini, M. Duquesne, A. Laigle, P. Y. Turpin, and P. Vigny, Appl. Spectrosc. **44,** 1047 (1990).
39. S. Chadha, W. H. Nelson, and J. F. Sperry, Rev. Sci. Instrum. **64,** 3088 (1993).
40. S. A. Asher and C. R. Johnson, *Science* **225,** 311 (1983)
41. J. Walker, Rep. Prog. Phys. **42,** 1605 (1979).
42. A. T. Tu, *Raman Spectroscopy in Biology* (Wiley, New York, 1982).
43. D. C. Blazej and W. L., Peticolas, Proc. Natl. Acad. Sci. USA **74,** 2639 (1977).
44. M. Majoube, P. Millie, P. Lagant, and G. Vergoten, J. Raman Spectrosc. **25,** 821 (1994).